# A fast algorithm for precise energy-loss calculations of high-energetic heavy ions

J. Benlliure [a], E. Casarejos [a], D. Cortina-Gil [a], E. Hanelt [b 1], M.F. Ordóñez [a], K.-H. Schmidt [b]

[a] *Universidad de Santiago de Compostela, 15706 Santiago de Compostela, Spain*

[b] *Gesellschaft für Schwerionenforschung, Planckstr. 1, 64291 Darmstadt, Germany*

Motivated by the need of precise energy-loss predictions to identify heavy reaction products, several computer codes to calculate the energy loss of high-energetic heavy ions are tested. Some of them are found to deviate strongly, in some cases more than 10%, from the available experimental data. A new algorithm is presented which is particularly suited for technical applications. It combines high precision with very short computing times.

*Key words:* Stopping powers; model calculations; high-energetic heavy ions; isotope identification and separation in magnetic spectrometers
*PACS:* 34.50.Bw, 29.30.Aj

## 1 Introduction

High-energetic heavy ions are largely used in both fundamental research and applications. An example of investigations with relativistic heavy ions is the production and study of exotic nuclei [1] while one of the most outstanding applications is the tumour radiotherapy with heavy ions [2]. A common need to all these investigations is a detailed knowledge of the atomic interactions of relativistic heavy ions with matter. In particular, accurate energy-loss calculations are strongly demanded.

In the case of fundamental research with heavy ions, in-flight separators allow to identify isotopically the reaction residues by means of the so called

[1] Present address: Konsorcium für Elektro-chemische Industrie GmbH, Zielstatt-Strasse 20 81379 München, Germany

momentum-loss achromat method ($B\rho - \Delta p$) [3,4]. This technique is used for the production and separation of radioactive nuclear beams in projectile-fragmentation reactions. Recently, this method was also applied for detailed investigations of spallation reactions at GSI [5–8]. These reactions have a large interest in nuclear astrophysics, but they are also considered as an optimal neutron source for material-science investigation [9] or for the transmutation of nuclear waste [10,11].

These experiments take profit of the inverse kinematics where all the reaction residues are emitted in the forward direction. The high resolution in-flight separator Fragment Separator (FRS) [12] was used to identify isotopically all those reaction residues. The unambiguous identification of the heavier reaction residues was done using the $B\rho - \Delta p$ which relies on a precise determination of the energy loss of the reaction residues.

Several codes (GEANT [14], SRIM [15], ATIMA [16]) are able to estimate the energy loss of relativistic heavy ions. However, some of them have been developed for the interaction of light particles with matter and their validity to estimate accurately the energy loss of heavy ions could be under question. Other codes like ATIMA [16] treat specifically the energy loss of relativistic heavy ions but certain applications can not afford for the computing times of such codes.

In the present work, we compare the predictive power of several standard codes for the evaluation of the energy loss for relativistic heavy ions. In addition, we present a new algorithm for this application which combines high precision with very short computing times.

## 2 Energy-loss calculations for a momentum-loss achromat.

In this chapter we discuss the accuracy of the energy-loss calculations, which is required for separating and identifying secondary beams in a momentum-loss achromat as an example for a technical application. A two-stage magnetic achromatic system, equipped with a profiled energy degrader in its intermediate image plane, has been introduced to provide an isotopically separated beam of reaction residues produced in peripheral collisions of heavy ions [3,4]. An example of a momentum-loss achromat is provided in Fig. 1 where a schematic view of the FRS at GSI is shown [12].

The two stages of the momentum-loss achromat, from the target to the intermediate image plane $F2$ and from $F2$ to the exit, provide the isotopic separation of the reaction residues. In the image plane behind the first stage, a selection according to the momentum-over-charge ratio is made. For isotopes

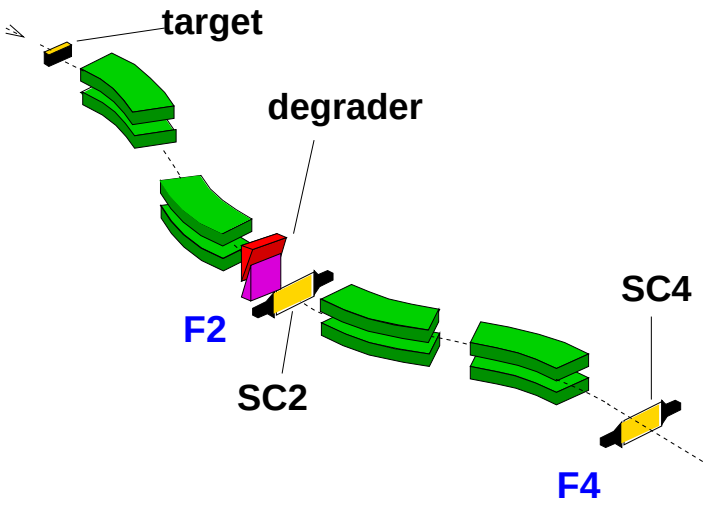


Fig. 1. Schematic view of the FRS magnetic spectrometer at GSI. This two-stages achromatic spectrometer with a profiled intermediate degrader provides the conditions to separate ions according to the momentum-loss achromat method. Two plastic scintillators ($SC2$, $SC4$) placed at the intermediate $F2$ and final $F4$ images planes, respectively, provide the position of the ions at both image planes in the direction of the dispersion.

with a sufficiently narrow velocity distribution, this selection is mainly determined by the A/Z ratio. For a complete isotopic separation, an additional selection according to the atomic number is performed. For that purpose, a thick energy degrader is placed in front of the second stage of the spectrometer. In the second stage, the ions are deflected according to their residual momentum after the energy loss in the thick degrader, which is roughly proportional to their atomic charge squared. In order to preserve the achromaticity, the degrader is profiled in such a way that the ions lose a fixed fraction of their momentum, independent of their deflection in the first stage. These two selections are illustrated in Fig. 2, where a scatter plot of the horizontal positions in the two image planes is shown for the spallation products of $^{238}$U at 1 A GeV. Only a limited number of nuclides around $^{225}$Ra are transmitted.

The identification of the transmitted ions relies on accurate estimations of their magnetic rigidities in both sections of the spectrometer. The kinematic properties of the ions, entering into the spectrometer, are determined by the reaction mechanism by which they are produced as described in Ref. [17]. In peripheral collisions of relativistic heavy ions, the longitudinal velocities of the projectile residues are rather close to the initial velocity of the projectiles [18]. This determines the magnetic fields to be applied in the first stage of the separator for selecting reaction products with a specific A/Z ratio. The Z range of the reaction products to be selected in the second stage of the separator relies on an accurate knowledge of their energy loss in the energy degrader. For the heaviest nuclei around Z = 92, the energy loss of neighbouring elements differs by about 2%. For an unambiguous identification, the energy loss should

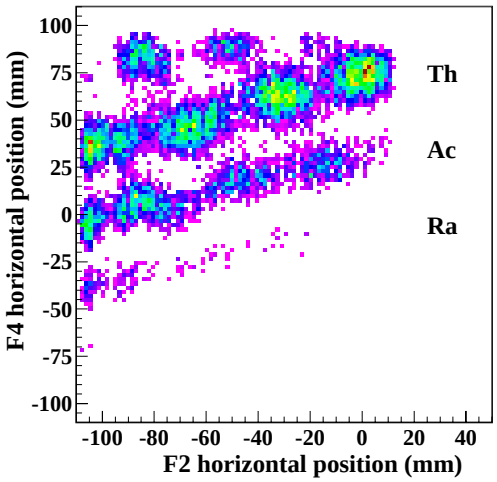


Fig. 2. Scatter plot of the correlation between the positions of the ions in the direction of the dispersion at the two image planes of the FRS obtained in a typical tuning of the spectrometer for the reaction $^{238}$U(1 A GeV)+d [13]. While the position of the ions at the intermediate image plane $F_2$ provides a separation according to their A/Z ratio, the position at the final image plane $F_4$ separates the ions according to their momentum loss in the intermediate thick degrader providing a selection in atomic number.

be known with an appreciably better precision in the order of 0.5%. In fact, a common normalisation of the calculation, e.g. due to the uncertainty in the thickness of the energy degrader, can be applied, if the calculated energy-loss values are normalised to a measured value, deduced from the magnetic rigidities of a known ion in the two stages of the separator. This normalisation can be determined by centring the projectile beam along the spectrometer.

We conclude that energy-loss calculations should have an accuracy of about 0.5% to provide an unambiguous identification of the heaviest secondary beams in a momentum-loss achromat. In order to reach this high accuracy, the calculations can be re-normalised with the measured energy loss of the primary projectiles. For a correct identification of nuclei far from the projectile, the calculated energy loss is required to preserve the necessary accuracy. Therefore, a realistic description of the energy loss as a function of the projectile and as a function of energy is most important for this application.

## 3 Standard codes for energy-loss calculations

The theoretical aspects of the energy-loss of relativistic heavy ions are extensively discussed in the review article of Ahlen [19]. Here we will just discuss

the main characteristics of some of the most used codes to calculate energy losses of relativistic heavy ions.

The code SRIM 2000 [15] consists of a package of programs to calculate the stopping powers and ranges of ions in matter in an energy range between 10 eV and 2 GeV using a quantum-mechanical treatment of the ion-atom collision. The code uses statistical algorithms which allow the ion to jump between calculated collisions and then to average the collision results over the considered interval. During the collisions, the ion and the target atoms interact by screened Coulomb collision, including exchange and correlations interactions between the overlapping electron shells. A detailed description of the calculation can be found in Refs. [20,21].

GEANT 3.21 is a complex software package from CERN which simulates the interaction and propagation of particles and radiation with matter. The code is able to simulate the dominant processes which can occur in the energy range from 10 keV to 10 TeV for electromagnetic interactions. By means of systematic fits to the existing data, the cross sections for electromagnetic processes are reproduced from 10 keV up to 100 GeV, both for light and for heavy materials. It computes the stopping powers for protons with a Bethe-Bloch formula using the semi-empirical shell-structure correction of Barkas [22] and density-effect corrections due to Sternheimer [23]. The used values of the ionisation potential are given in Ref. [24]. The stopping powers of heavy nuclei are then computed from proton stopping powers with a scaling expression. Charge-exchanges in the stopper material are taken into account with a semi-empirical formula of Anderson [24]. A full description of the code can be found in [14].

The code ATIMA, developed at GSI, Darmstadt, calculates several physical quantities characterizing the slowing-down of protons and heavy ions in matter for specific kinetic energies ranging from 50 A MeV to 500 A GeV. It computes stopping powers following closely the Lindhard and Sorensen theory [25] that takes into account the deviation of stopping power expressions from the first-order quantum perturbation theory. For further information see [16].

## 4 The new fast algorithm AMADEUS

Although the codes presented in the previous section are quite elaborated, often they require considerably long computing times to integrate the stopping powers. In addition, they are difficult to be introduced in more general computing programs requiring the evaluation of energy losses. An example is the evaluation of the fission kinematics in a recent inverse-kinematics experiment with secondary beams, for which the energy loss in a number of layers had to

be computed on an event-by-event basis for all individually measured fission fragments [26,27]. For this kind of application, we developed a semiempirical algorithm to evaluate energy losses in thick layers of matter following a fast and efficient procedure. The basic idea was to parameterise the range of ions in any material by using an analytical function that can be inverted. Then the energy loss in a layer of matter with thickness $d$ can be obtained as:

$$\Delta E(d) = E_i - E_f \tag{1}$$

where $E_i$ is the initial energy of the ion and $E_f$ is the remaining energy of the ion after traversing the layer of matter that can easily be calculated from the residual ranges before and behind the layer, $r(E_i)$ and $r(E_f)$, since

$$r(E_f) = r(E_i) - d \tag{2}$$

and the function $r(E)$ can be inverted.

To determine the function $r(E)$, first we calculated the range of a number of different projectile-stopper combinations by numerical integration of the stopping-power expressions presented in the appendix of Ref. [4]. Then we fitted the values in an energy range between 100 A MeV and 2 A GeV with the least squares method to the function:

$$r(Z_p, A_p, E/A_p) = k\,\frac{A_p}{Z_p^2}\,10^{\kappa} \qquad mg/cm^2 \tag{3}$$

where

$$\begin{aligned}\kappa = (1 + p_1 Z_p + p_2 Z_p^2 + p_3 Z_p^3 + p_4 Z_p^4) \cdot [(p_5 + p_6 Z_p) \\ +(p_7 + p_8 Z_p) log_{10}(E/A_p) + (p_9 + p_{10} Z_p) log_{10}^2(E/A_p)]\end{aligned} \tag{4}$$

with $A_p$ and $Z_p$ the mass and atomic number of the ion, respectively, and $E/A_p$ its energy in A MeV.

The set of parameters $p_1$ to $p_{10}$ resulting from the fit are listed in table 1 for Be, C and Al and in table 2 for Sn, Ta and Pb. The different sets of parameters were adjusted separately to each stopper material but simultaneously for 21 projectiles from $Z_p = 3$ to $Z_p = 92$ and for all energies between E/A = 100 MeV and 2 GeV.

The factor k in equation 3 allows to interpolate the calculation of the range

Table 1
Parameters $p_1$ to $p_{10}$ which provide the range of any ion with energy between 100 and 200 A MeV in Be, C and Al according to the expression 3.

| in Be (Z = 4) | in C (Z = 6) | in Al (Z = 13) |
|---|---|---|
| $p_1 = -1.28428 \cdot 10^{-4}$ | $6.67801 \cdot 10^{-4}$ | $-6.68659 \cdot 10^{-5}$ |
| $p_2 = -1.73612 \cdot 10^{-6}$ | $-3.92137 \cdot 10^{-6}$ | $-1.85311 \cdot 10^{-6}$ |
| $p_3 = 8.89892 \cdot 10^{-8}$ | $1.36917 \cdot 10^{-7}$ | $8.73192 \cdot 10^{-8}$ |
| $p_4 = -7.05115 \cdot 10^{-10}$ | $-9.72996 \cdot 10^{-10}$ | $-6.90141 \cdot 10^{-10}$ |
| $p_5 = -0.553492$ | $-0.490202$ | $-0.530758$ |
| $p_6 = 9.12049 \cdot 10^{-3}$ | $7.51599 \cdot 10^{-3}$ | $8.98953 \cdot 10^{-3}$ |
| $p_7 = 2.68184$ | $2.61390$ | $2.68916$ |
| $p_8 = -0.210108 \cdot 10^{-3}$ | $-6.00822 \cdot 10^{-3}$ | $-5.33772 \cdot 10^{-3}$ |
| $p_9 = 7.74360 \cdot 10^{-4}$ | $-0.199549 \cdot 10^{-4}$ | $-0.214131$ |
| $p_{10} = -1.28428 \cdot 10^{-4}$ | $7.31880 \cdot 10^{-4}$ | $7.73008 \cdot 10^{-4}$ |

to other stopping materials than those used for the fit. This factor can be obtained from the following relations:

$$
\begin{aligned}
0 < Z_t \leq 5: &\quad k = A_t/9.012 \cdot (4/Z_t)^{0.98} \\
5 < Z_t \leq 9: &\quad k = A_t/12.011 \cdot (6/Z_t)^{0.98} \\
9 < Z_t \leq 32: &\quad k = A_t/26.982 \cdot (13/Z_t)^{0.90} \\
32 < Z_t \leq 64: &\quad k = A_t/118.69 \cdot (50/Z_t)^{0.88} \\
64 < Z_t \leq 72: &\quad k = A_t/180.95 \cdot (73/Z_t)^{0.88} \\
72 < Z_t \leq 92: &\quad k = A_t/207.20 \cdot (82/Z_t)^{0.80}
\end{aligned}
$$

where $A_t$ and $Z_t$ represent the mass and the atomic numbers of the stopping material, respectively. When the stopping material is a mixture of different isotopes, the mean mass number has to be used for $A_t$.

A more accurate determination of the range can be obtained by applying the correction factor $F_{corr}$ to the equation 3:

$$
r(Z_p, A_p, E/A_p) = k \, \frac{A_p}{Z_p^2} \, 10^{\kappa} \cdot F_{corr} \qquad mg/cm^2 \tag{5}
$$

Table 2
Parameters $p_1$ to $p_{10}$ which provide the range of any ion with energy between 100 and 200 A MeV in Sn, Ta and Pb according to the expression 3.

| in Sn (Z = 50) | in Ta (Z = 73) | in Pb (Z = 82) |
|---|---|---|
| $p_1 = 1.23639 \cdot 10^{-3}$ | $-1.99249 \cdot 10^{-5}$ | $-3.75861 \cdot 10^{-4}$ |
| $p_2 = -6.13893 \cdot 10^{-6}$ | $-2.27944 \cdot 10^{-6}$ | $-3.73902 \cdot 10^{-6}$ |
| $p_3 = 1.84116 \cdot 10^{-7}$ | $1.05063 \cdot 10^{-7}$ | $1.48861 \cdot 10^{-7}$ |
| $p_4 = -1.20551 \cdot 10^{-9}$ | $-8.29122 \cdot 10^{-10}$ | $-1.12159 \cdot 10^{-9}$ |
| $p_5 = -0.263421$ | $-0.325062$ | $-0.166220$ |
| $p_6 = 6.34349 \cdot 10^{-3}$ | $9.75017 \cdot 10^{-3}$ | $1.26920 \cdot 10^{-2}$ |
| $p_7 = 2.61081$ | $2.68814$ | $2.59061$ |
| $p_8 = -6.38315 \cdot 10^{-3}$ | $-6.07419 \cdot 10^{-3}$ | $-7.25322 \cdot 10^{-3}$ |
| $p_9 = -0.204813$ | $-0.218986$ | $-0.202004 \cdot 10^{-4}$ |
| $p_{10} = 6.63267 \cdot 10^{-4}$ | $8.69283 \cdot 10^{-4}$ | $1.17942 \cdot 10^{-3}$ |

with

$$F_{corr} = 1/(0.965735686 + 9.79114E-03 \cdot R + 3.17099E-03 \cdot R^2 \\ -6.71227E-04 \cdot R^3 + 2.28409E-05 \cdot R^4) \quad (6)$$

where $R = Z_p^2/1000$

This analytical range-energy relation (5) can be inverted according to the following equation:

$$E(Z_p, A_p, r) = 10^{\frac{-(p_7+p_8 Z_p)}{2(p_9+p_{10}Z_p)}} - \sqrt{\left(\frac{(p_7+p_8 Z_p)}{2(p_9+p_{10}Z_p)}\right)^2 - \frac{p_5+p_6 Z_p}{p_9+p_{10}Z_p}} \\ + \frac{log_{10}(\frac{r/F_{corr}}{kZ^2/A})}{(1+p_1 Z_p + p_2 Z_p^2 + p_3 Z_p^3 + p_4 Z_p^4)(p_9+p_{10}Z_p)} \quad (7)$$

Expressions 5 and 7 allow us to calculate analytically the range and energy of any ion traversing any stopping material, and together with equations 1 and 2 we can determine their energy loss. Therefore, these analytical range-

energy relations constitute a very fast algorithm for energy-loss calculations, well suited for technical applications.

The analytical range-energy relations provide another important advantage: The fact that the functions (5) and (7) are the exact inverse functions of each other avoids systematical inconsistencies which could occur if tabulated range values are interpolated. This was an essential requirement for the evaluation of the fission kinematics in the experiment mentioned above [26,27].

The applicability of the description 5 and 7 is restricted to energies between 100 A MeV and 2 A GeV. In particular, we do not expect that the complex behaviour at lower energies is correctly reproduced.

## 5 Comparison with experimental data

In order to validate some of the codes mostly used to evaluate energy losses at relativistic heavy ions and the new algorithm presented in this work, in this section we compare the results obtained using these codes with a set of available experimental measurements on energy losses [28–32]. The results are given in tables 3, 4 and 5.

From this comparison we can deduce that ATIMA seems to provide the better description of the experimental data. AMADEUS provides also a description of the experimental data within a few percent accuracy. However, this good agreement does not exist in the cases of GEANT 3.21 and SRIM 2000 codes, at least, for heavy projectiles. For light projectiles the predictions of both codes are in quite good agreement with the measured data. In contrast, for mass numbers beyond A = 86 the relative differences are systematically larger than the experimental errors. This behaviour is specially notable in the uranium region, where the relative differences are close to 10% and even larger when we consider heavy target materials.

To quantify the predictive power of the different codes we have used the sum of quadratic deviations, normalised by the number of data points as given by the following expression:

$$M = \frac{\sum \left( \frac{\Delta E^i_{data} - \Delta E^i_{cal}}{\Delta Err^i_{data}} \right)^2}{n} \tag{8}$$

In this equation $\Delta E_{data}$ and $\Delta E_{cal}$ represent the measured and calculated energy losses, respectively, and $\Delta Err_{data}$ is the uncertainty of the measured

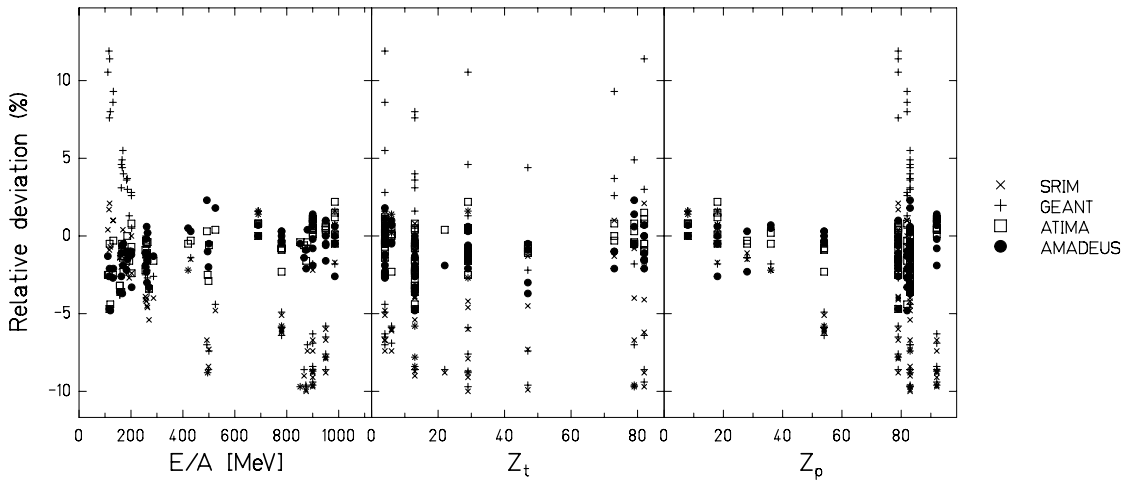


Fig. 3. Relative deviations of the different model descriptions from the measured energy-loss values as a function of energy $E$, target element $Z_t$ and projectile element $Z_p$.

energy losses. $n$ represents the number of experimental measurements considered to evaluate $M$.

The results were $M = 3.5$ for ATIMA, $M = 4.2$ for AMADEUS, $M = 57.6$ for GEANT 3.21 and $M = 48.7$ for SRIM 2000. As already mentioned, the best agreement to the data is obtained with the code ATIMA. AMADEUS provides very similar results. However, the predictions of GEANT 3.21 and SRIM 2000 are quite far from an overall good description of the measured energy losses. Consequently, we can conclude that these two codes are not suitable to compute energy losses of high-energetic heavy ions with the accuracy required for some applications as the isotope identification in peripheral collisions of relativistic heavy ions with a magnetic spectrometer.

The deviations of the model descriptions from the experimental data can be analysed in more detail on the basis of the graphical presentation as function of energy, target and projectile shown in Fig. 3. There is a clear tendency of GEANT 3.21 to overpredict the energy loss of heavy ions at low energies below 200 A MeV. Moreover, the values for energies above 400 A MeV are underpredicted by both, GEANT 3.21 and SRIM 2000. These deviations seem predominantly to occur for the most heavy projectiles. There is no systematic tendency of the deviations of any of the models as a function of the target element. The deviations of ATIMA and AMADEUS do not exceed the values expected from the uncertainties of the experimental data.

The energy-loss calculations performed with ATIMA or AMADEUS seem also to be best suited for the isotopic identification of secondary beams in a momentum-loss achromat which was discussed in chapter 2. The uncertain-

ties of the experimental data do not allow to decide whether the required accuracy of 0.5% can be reached. However, the fact that there are no systematic trends observed in the deviations of these two descriptions from the experimental values as a function of energy or nuclear charge of the projectile might give some confidence that the required accuracy can be reached after renormalising the calculation to the measured energy loss of the projectile. The systematic trends in the deviations of the other descriptions, SRIM 2000 and GEANT 3.21, as shown in Fig. 3 clearly indicate that these are not suited for this application.

## 6 Conclusion

The accurate determination of the energy loss of high-energetic heavy ions in matter is crucial in fundamental experimental research on nuclear dynamics and structure as well as in many applications like tumour radiotherapy with heavy ions. In particular in this work we show that the accuracy needed in energy-loss calculations to identify heavy-exotic nuclei produced in peripheral collisions of relativistic heavy ions is of the order of few percent.

The comparison of some commonly used codes for energy-loss calculation with measured data show that some of them, like the code ATIMA, provide a good description of the data while some others, like GEANT 3.21 or SRIM 2000, are far from the required accuracies, especially when we consider heavy projectiles and heavy target materials.

Since many of the available codes are quite time consuming and they can not be integrated easily in more general computing programs requiring the evaluation of energy losses we developed a new fast algorithm to evaluate energy losses of high-energetic heavy ions in thick layers, AMADEUS. This algorithm is based on a parameterisation of the range of heavy ions in any material by using an analytical function that can be inverted. The results obtained with this algorithm are similar to the ones given by the ATIMA code although the present formulation is limited to an energy range between 100 A MeV and 2 A GeV.

## 7 Acknowledgement

The authors would like to thank H. Weick for valuable discussions. This work was partially supported by the European Commission under programme "Access to Research Infrastructure Action of the Improving Human Potential" contract n. HPRI-1999-CT-00001 and by the "Secretaría Xeral de In-

vestigación e Desenvolvemento da Xunta de Galicia" under contract number PGIDT00PXI20606PM.

## References

[1] NuPECC Report "The NuPECC Working Group on Radioactive Beam Facilities", April 2000

[2] G. Kraft Strahlenther. Onkol. 166 (1990) 10

[3] J.-P. Dufour, R. Del Moral, H. Emmermann, F. Huber, D. Jean, C. Poinot, M. S. Pravikoff, A. Fleury, H. Delagrange, K.-H. Schmidt, Nucl. Instr. and Methods A 248 (1986) 267

[4] K.-H. Schmidt, E. Hanelt, H. Geissel, G. Müenzenberg, J.-P. Dufour, Nucl. Instr. and Methods A 260 (1987) 287

[5] W. Wlazlo, T. Enqvist, P. Armbruster, J. Benlliure, M. Bernas, A. Boudard, S. Czajkowski, R. Legrain, B. Mustapha, M. Pravikoff, F. Rejmund, K.-H. Schmidt, C. Stephan, J. Taieb, L. Tassan-Got, C. Volant, Phys. Rev. Lett. 84 (2000) 5736

[6] J. Benlliure, P. Armbruster, M. Bernas, A. Boudard, J. P. Dufour, T. Enqvist, R. Legrain, S. Leray, B. Mustapha, F. Rejmund, K.-H. Schmidt, C. Stphan, L. Tassan-Got, C. Volant, Nucl. Phys. A 683 (2001) 513

[7] F. Rejmund, B. Mustapha, P. Armbruster, J. Benlliure, M. Bernas, A. Boudard, J. P. Dufour, T. Enqvist, R. Legrain, S. Leray, K.-H. Schmidt, C. Stphan, J. Taieb, L. Tassan-got, C. Volant, Nucl. Phys. A 683 (2001) 540

[8] T. Enqvist, W. Wlazlo, P. Armbruster, J. Benlliure, M. Bernas, A. Boudard, S. Czajkowski, R. Legrain, S. Leray, B. Mustapha, M. Pravikoff, F. Rejmund, K.-H. Schmidt, C, Stephan, J. Taieb, L. Tassan-Got, C. Volant, Nucl. Phys. A 686 (2001) 481

[9] *The European Spallation Source Study, vol.III*, The ESS Technical Study, report ESS-96-53-M (1996)

[10] C.D. Bowman, E.D. Arthur, P.W. Lisowski, G.P. Lawrence, R.J. Jensen, J.L. Anderson, B. Blind, M. Cappiello, J.W. Davidson, T.R. England, L.N. Engel, R.C. Haight, H.G. Hughes III, J.R. Ireland, R.A. Krakowski, R.J. LaBauve, B.C. Letellier, R.T. Perry, G.J. Russel, K.P. Staudhammer, G. Versamis, W.B. Wilson, Nucl. Instr. and Methods A 320 (1992) 336

[11] T.Takizuka, *Proc. of the International Conference on Accelerator-Driven Transmutation Techonologies and Applications*, Las Vegas (1994)

[12] H. Geissel, P. Armbruster, K.-H. Behr, A. Bruenle, K. Burkard, M. Chen, H. Folger, B. Franczak, H. Keller, O. Klepper, B. Langenbeck, F. Nickel, E.

Pfeng, M. Pfützner, E. Roeckl, K. Rykaczewsky, I. Schall, D. Schardt, C. Scheidenberger, K.-H. Schmidt, A. Schroeter, T. Schwab, K. Sümmerer, M. Weber, G. Münzenberg, T. Brohm, H.-G.Clerc, M. Fauerbach, J.-J. Gaimard, A. Grewe, E. Hanelt, B. Knoedler, M. Steiner, B. Voss, J. Weckenmann, C. Ziegler, A. Magel, H. Wollnik, J.-P. Dufour, Y. Fujita, D. J. Vieira, B. Sherrill, Nucl. Instr. and Methods B 70 (1992) 286

[13] E. Casarejos Phd, Universidad de Santiago de Compostela 2001

[14] http://wwwinfo.cern.ch/asd/geant/index.html

[15] http://www.SRIM.org/

[16] http://www-aix.gsi.de/ scheid/ATIMA1.html

[17] J. Benlliure, J. Pereira-Conca, K.-H. Schmidt, Nucl. Instr. and Methods A, in print

[18] D.J. Morrissey, Phys. Rev. C 39 (1989) 460

[19] S.P. Ahlen, Rev. Mod. Phys. 52 (1980) 121

[20] J. P. Biersack and L. Haggmark, Nucl. Instr. and Methods A 174 (1980) 257

[21] J.F. Ziegler, J.P. Biersack and U. Littmark, Pergamon Press, New York (1996)

[22] W.H. Barkas. Technical report 10292, UCRL, August 1962.

[23] R.M. Sternheimer Phys. Rev. 88 (1962) 851

[24] H.H. Andersen and J.F. Ziegler. *Hydrogen stopping powers and ranges in all elements*. Pergamon Press, 1977.

[25] J. Lindhard, A.H. Sorensen, Phys. Rev. A 53 (1996) 2443

[26] C. Böckstiegel, S. Steinhäuser, J. Benlliure, H.-G. Clerc, A. Grewe, A. Heinz, M. de Jong, A. R. Junghans, J. Müller, K.-H. Schmidt, Phys. Lett. B 398 (1997) 259

[27] K.-H. Schmidt, S. Steinhäuser, C. Böckstiegel, A. Grewe, A. Heinz, A. R. Junghans, J. Benlliure, H.-G. Clerc, M. de Jong, J. Mueller, M. Pfützner, B. Voss, Nucl. Phys. A 665 (2000) 221

[28] C. Scheidenberger, H. Geissel, H.H. Mikkelsen, F. Nickel, T. Brohm, H. Folger, H. Irnich, A. Magel, M.F. Mohar, G. Münzenberg, M. Pfützner, E. Roeckl, I. Schall, D. Schardt, K.-H. Schmidt, W. Schwab, M. Steiner, Th. Stöhlker, K. Sümmerer, D.J. Vieira, B. Voss, M. Weber, Phys. Rev. Lett. 73 (1994) 50

[29] C. Scheidenberger Phd, Jüstüs-Liebig Universität Giessen 1994.

[30] H. Weick, H. Geissel, C. Scheidenberger, F. Attallah, T. Baumann, D. Cortina, M. Haussmann, B. Lommel, G. Münzenberg, N. Nankov, F. Nickel, T. Radon, H. Schatz, K. Schmidt, J. Stadlmann, K. Sümmerer, M. Winkler, H. Wollnik, Nuc. Instr. and Methods B 164 (2000) 168

[31] H. Weick, H. Geissel, C. Scheidenberger, F. Attallah, D. Cortina, M. Haussmann, G. Münzenberg, T. Radon, H. Schatz, K. Schmidt, J. Stadlmann, K. Sümmerer, M.Winkler, Phys. Rev. Lett. 85 (2000) 2725.

[32] H. Weick Phd, Jüstüs-Liebig Universität Giessen 2000.

Table 3
Comparison between measured stopping powers (dE/$\rho$dx) from Ref. [28,29] and the calculated ones with different codes. The comparison with the calculated stopping powers is shown as relative values to the measured data in percent. The uncertainties of the measured stopping powers are also given in relative as percentage inside the parenthesis.

| Projectile(A MeV) | Target | dE/$\rho$dx(MeV/mg/cm$^2$) | AMADEUS | ATIMA | GEANT | SRIM |
|---|---|---|---|---|---|---|
| $^{18}O$(690) | Be | 0.125(1.6) | 0.0 | 0.8 | 1.6 | 1.6 |
| | C | 0.138(2.9) | 0.7 | 0.0 | 1.4 | 1.4 |
| | Al | 0.123(3.2) | 0.0 | 0.8 | 1.6 | 0.8 |
| $^{40}Ar$(985) | Be | 0.587(2.7) | -0.5 | 1.2 | 0.7 | 0.7 |
| | C | 0.640(2.9) | -0.5 | 0.1 | 0.2 | 0.2 |
| | Al | 0.584(3.2) | -2.6 | -0.5 | -1.8 | -1.7 |
| | Cu | 0.494(3.2) | 0.6 | 2.2 | 1.6 | 1.6 |
| | Pb | 0.389(3.1) | 0.0 | 1.5 | 0.7 | 0.7 |
| $^{58}Ni$(260) | Be | 2.477(2.5) | -2.3 | -0.5 | -1.4 | -1.1 |
| 430 | Be | 1.904(2.0) | 0.3 | -0.3 | -1.4 | -1.5 |
| $^{86}Kr$(420) | Be | 3.206(1.5) | 0.5 | -0.5 | -2.2 | -2.2 |
| 900 | Be | 2.432(1.5) | 0.7 | 0.2 | -1.8 | -2.2 |
| $^{136}Xe$(780) | Be | 5.861(1.3) | 0.3 | -0.9 | -4.9 | -5.1 |
| | C | 6.524(1.3) | -0.4 | -2.3 | -5.9 | -6.1 |
| | Al | 5.806(2.1) | -0.3 | -0.8 | -5.8 | -5.8 |
| | Cu | 5.077(1.3) | 0.3 | -0.8 | -5.9 | -6.0 |
| | Pb | 3.959(1.6) | 0.0 | -0.5 | -6.4 | -6.2 |
| $^{197}Au$(950) | Be | 12.124(1.0) | 0.0 | 0.2 | -6.5 | -6.7 |
| | C | 13.256(1.2) | 1.0 | 0.6 | -5.8 | -6.0 |
| | Al | 12.086(1.3) | -0.5 | 0.4 | -7.8 | -7.8 |
| | Cu | 10.572(1.2) | -0.6 | 0.5 | -7.6 | -7.9 |
| | Pb | 8.332(1.2) | -1.6 | 0.8 | -8.6 | -8.8 |
| $^{209}Bi$(157) | Al | 27.406(3.5) | -3.6 | -3.2 | -3.8 | -1.4 |
| $^{238}U$(900) | Be | 16.648(1.1) | 1.1 | 1.1 | -6.3 | -6.7 |
| | C | 18.470(1.5) | 0.7 | 0.1 | -6.9 | -7.4 |
| | Al | 16.739(1.0) | -0.2 | 0.5 | -8.4 | -8.7 |
| | Ti | 15.379(1.5) | -1.9 | 0.4 | -8.6 | -8.8 |
| | Cu | 14.703(1.1) | -0.8 | 0.4 | -8.7 | -9.1 |
| | Au | 11.728(1.5) | 1.4 | 0.8 | -9.6 | -9.6 |
| | Pb | 11.533(1.8) | 0.7 | 1.1 | -9.4 | -9.7 |

Table 4
Comparison between measured stopping powers (dE/$\rho$dx) from Ref. [30–32] and the calculated ones with different codes. The comparison with the calculated stopping powers is shown as relative values to the measured data in percent. The uncertainties of the measured stopping powers are given in relative as percentage inside the parenthesis.

| Projectile(A MeV) | Target | dE/$\rho$dx(MeV/mg/cm$^2$) | AMADEUS | ATIMA | GEANT | SRIM |
|---|---|---|---|---|---|---|
| $^{197}Au$(115.3) | Be | 30.34(1.0) | -2.6 | -2.5 | 11.9 | 1.7 |
| 257.7 | Be | 19.54(0.7) | -0.2 | -0.3 | 0.0 | -1.4 |
| 117.0 | Al | 29.56(1.0) | -4.7 | -4.7 | 7.6 | -0.9 |
| 255.7 | Al | 19.49(0.7) | -1.9 | -2.2 | -2.5 | -3.9 |
| 286.7 | Al | 18.36(3.3) | -1.3 | -1.6 | -2.6 | -4.0 |
| 110.9 | Cu | 25.56(1.3) | -1.3 | -2.5 | 10.54 | 0.4 |
| 263.4 | Cu | 16.62(1.1) | -1.6 | -1.5 | -2.7 | -4.6 |
| 117.6 | Pb | 18.11(1.3) | -2.1 | -0.5 | 11.4 | 2.1 |
| 255.5 | Pb | 12.75(0.9) | -1.1 | -0.9 | -2.1 | -4.1 |
| $^{208}Pb$(130.7) | Be | 30.35(1.0) | -2.7 | -2.5 | 8.6 | 1.0 |
| 201.8 | Be | 23.79(0.5) | -1.2 | -0.7 | 2.8 | -0.0 |
| 120.4 | Al | 31.02(0.6) | -4.8 | -4.4 | 8.0 | -0.7 |
| 202.6 | Al | 23.45(0.6) | -3.3 | -2.4 | 0.5 | -2.4 |
| 193.3 | Cu | 20.64(0.6) | -1.3 | -1.6 | 1.3 | -2.7 |
| 132.2 | Ta | 19.12(1.3) | -2.1 | -0.3 | 9.3 | 1.0 |
| 201.8 | Ta | 15.56(0.6) | -1.0 | 0.8 | 2.6 | -1.0 |
| $^{209}Bi$(168.8) | Be | 26.84(0.8) | -1.9 | -1.4 | 5.5 | 0.4 |
| 264.0 | Be | 21.27(1.2) | 0.2 | -0.4 | 0.2 | -1.6 |
| 525.1 | Be | 15.81(0.8) | 1.8 | 0.4 | -4.4 | -4.8 |
| 879.6 | Be | 13.73(0.6) | 0.4 | -0.4 | -7.0 | -7.4 |
| 157 | Al | 27.41(3.5) | -3.6 | -3.2 | -3.8 | -1.4 |
| 162.8 | Al | 27.03(0.7) | -2.6 | -3.6 | 3.1 | -2.0 |
| 171.0 | Al | 26.04(2.5) | -0.5 | -2.3 | 4.0 | -1.1 |
| 183.0 | Al | 25.01(2.5) | -2.2 | -1.6 | 3.6 | -1.0 |
| 269.6 | Al | 21.18(1.5) | -3.3 | -3.4 | -3.6 | -5.4 |
| 498.6 | Al | 16.42(0.5) | -2.0 | -2.9 | -8.6 | -8.4 |
| 866.7 | Al | 13.78(0.5) | -1.4 | -0.6 | -8.6 | -9.0 |
| 163.3 | Cu | 22.82(0.9) | -1.1 | -1.3 | 4.6 | -1.1 |

Table 5
Same as table 4.

| Projectile(A MeV) | Target | dE/$\rho$dx(MeV/mg/cm$^2$) | AMADEUS | ATIMA | GEANT | SRIM |
|---|---|---|---|---|---|---|
| $^{209}Bi$(258.8) | Cu | 18.38(1.1) | -1.1 | -1.2 | -2.0 | -4.2 |
| 495.2 | Cu | 14.36(0.6) | -1.0 | -2.5 | -8.8 | -8.8 |
| 874.7 | Cu | 12.17(0.6) | -2.1 | -1.6 | -9.7 | -10.0 |
| 166.5 | Ag | 20.39(0.9) | -3.7 | -1.0 | 4.4 | -1.3 |
| 261.6 | Ag | 16.58(1.2) | -3.0 | -1.1 | -2.2 | -4.5 |
| 500.1 | Ag | 12.81(0.5) | -0.5 | -0.6 | -7.4 | -7.3 |
| 873.4 | Ag | 11.11(0.5) | -0.9 | -0.8 | -9.6 | -9.9 |
| 185.6 | Ta | 16.67(1.1) | -1.0 | 0.0 | 3.7 | -1.3 |
| 165.8 | Au | 17.25(0.8) | -0.6 | -0.5 | 4.9 | -0.8 |
| 260.4 | Au | 14.12(1.1) | 0.6 | -0.5 | -1.8 | -4.0 |
| 492.3 | Au | 11.03(0.5) | 2.3 | 0.3 | -7.0 | -6.7 |
| 851.6 | Au | 9.66(0.4) | -0.5 | -0.4 | -9.7 | -9.7 |
| 186.4 | Pb | 16.12(1.2) | -1.5 | -1.0 | 3.0 | -2.0 |